

$^{235}\text{U}(\text{n}, \text{f})$ Independent Fission Product Yield and Isomeric Ratio Calculated with the Statistical Hauser-Feshbach Theory

Shin Okumura^{1*}, Toshihiko Kawano², Patrick Talou², Patrick Jaffke², and Satoshi
Chiba¹

¹Laboratory for Advanced Nuclear Energy, Tokyo Institute of Technology, 2-12-1 Ookayama, Meguro-ku,
Tokyo 152-8550, Japan.; ²Theoretical Division, Los Alamos National Laboratory, Los Alamos, NM
87545, USA

We have developed a Hauser-Feshbach fission fragment decay model, HF³D, which can be applied to the statistical decay of more than 500 primary fission fragment pairs (1,000 nuclides) produced by the neutron induced fission of ^{235}U . The fission fragment yield $Y(A)$ and the total kinetic energy TKE are model inputs, and we estimate them from available experimental data for the $^{235}\text{U}(\text{n}_{\text{th}}, \text{f})$ system. The model parameters in the statistical decay calculation are adjusted to reproduce some fission observables, such as the neutron emission multiplicity $\bar{\nu}$, its distribution $P(\nu)$, and the mass dependence $\bar{\nu}(A)$. The calculated fission product yield and isomeric ratio are compared with experimental data. We show that the calculated independent fission product yield $Y_I(A)$ at the thermal energy reproduces the experimental data well, while the calculated isomeric ratios tend to be lower than the Madland-England model prediction. The model is extended to higher incident neutron energies up to the second chance fission threshold. We demonstrate for the first time that most of the isomeric ratios stay constant, although the production of isomeric state itself changes as the incident energy increases.

Keywords: Nuclear Fission, Statistical Decay, Isomeric Ratio, Fission Product Yield

1. Introduction

Thermal neutron induced fission, such as the $^{235}\text{U}(\text{n}_{\text{th}},\text{f})$ or $^{239}\text{Pu}(\text{n}_{\text{th}},\text{f})$ reactions, produces roughly 800 primary fission fragments¹. Since these fission fragments are highly excited, they de-excite by emitting several prompt neutrons and γ rays to reach their ground or metastable states within a time-scale of compound nucleus in the fission process. The independent fission product yield $Y_I(Z, A)$, which is a distribution of nuclides after emission of the prompt particles but before beta decay, plays an important role in many applications such as estimation of decay heat²⁻⁴ and delayed neutron emission^{5,6} in nuclear reactors, the reactor neutrino study⁷, prediction of fission product inventory at each stage of the nuclear fuel cycle, the radio-isotope production for medical applications, development of advanced reactor and transmutation systems, fission in the galactic chemical evolution⁸, and so on. A demand for high quality data of fission product yield (FPY) in such applications is rapidly increasing. New applications may require accurate FPY data at several neutron incident energies, while the current evaluated FPY data files contain only three energy points; the thermal, fast and 14-MeV incident energies, with an exception of the ^{239}Pu file in the evaluated nuclear data file, ENDF/B-VII.1⁹, where two energy points (0.5 and 2 MeV) are given in the fast range¹⁰.

Significant efforts have been made to compile the FPY experimental data and evaluation for the nuclear data libraries in the past. England and Rider¹ evaluated the FPY data for 60 fissioning systems in 1994, and released their results as part of ENDF/B-VI. They calculated $Y_I(Z, A)$ by combining the evaluated mass chain yield and the charge distribution in the most probable charge (Z_p) model proposed by Wahl¹¹. The FPY eval-

*Corresponding author. Email: okumura.s.aa@m.titech.ac.jp

uation in Japanese Evaluated Nuclear Data Library (JENDL/FPY-2011)^{12,13} followed the procedure of England and Rider, and these FPY data were upgraded by including new experimental FPY and making it consistent with the updated JENDL decay data library (JENDL/FPD-2011)¹².

The isomeric ratio data in both libraries are estimated by introducing the Madland and England (ME) model^{14,15}, whenever the isomeric ratio is experimentally unknown. Relative population of the isomeric and ground states in a fission product (after prompt neutron emission) is calculated by looking at the difference in their spins. An even-odd effect in the fission products is also considered. While this model is widely used in the current libraries, recent advances in the fission model together with the statistical Hauser-Feshbach decay^{16,17} could also be able to improve the evaluation of FPY data.

Despite many theoretical studies on fission that have been made in the past, prediction and reproduction of all the fission observables in a consistent manner are still challenging. A modeling of de-excitation of fission fragments requires many physical quantities¹⁸ that define an initial configuration of the fragment decay, such as the fragment excitation energy, spin-parity distribution, and (Z, A) distribution of primary fission fragments. The model predicts prompt particle emission probabilities and multiplicities, and $Y_I(Z, A)$ simultaneously by integrating over the distribution of initial configurations. Instead of performing the integration, several Monte Carlo (MC) tools have been developed to calculate the fission de-excitation process and to reproduce these observables¹⁸⁻²³. Although the MC technique gives correlations in the prompt particle emissions in fission, and it facilitates experimental data analysis by emulating directly the measurement set-up, its lengthy computation makes it difficult to fine-tune their model parameters. In addition, when a probability of fission fragment production is extremely small, the MC technique never samples such a case in a reasonable computational time. Because FPY varies in the order of magnitude, *e.g.* typically from 10^{-12} to 10^{-2} given in the evaluated files, the MC

technique is not an efficient method to be adopted in the FPY evaluation, and one has to migrate to a deterministic method, in which all the possible fission fragments can be included.

Our approach is to develop a new method to evaluate $Y_I(Z, A)$ by applying the deterministic technique for the primary fission fragment decay. The outline of our method is similar to our past study¹⁶, albeit no MC sampling is performed anymore. We apply the Hauser-Feshbach statistical decay to about 500 primary fission fragment pairs (1000 nuclides), and abbreviate this as HF³D (Hauser-Feshbach Fission Fragment Decay). Since the spin and parity conservation is naturally involved in the HF³D model, the isomeric ratio calculation is just straightforward¹⁷. The mass distribution of the primary fission fragment is represented by five Gaussians, and the Gaussian parameters are fitted to experimental data of $^{235}\text{U}(n_{\text{th}}, f)$. We use Wahl's Z_p model for the charge distribution. The experimental data of average prompt neutron multiplicity $\bar{\nu}$, its distribution $P(\nu)$, the mass dependence $\bar{\nu}(A)$, and the total kinetic energy (TKE) are taken into account to constrain our model parameters. A dynamical treatment of fission process such as the Langevin model²⁴⁻²⁹ or a random walk technique³⁰⁻³² is able to provide some of our inputs such as TKE and/or $Y(Z, A)$ distribution. These dynamical models could be used when their predictive capability meets required accuracy of the evaluated FPY data. At this moment we stay on a phenomenological approach and rely more on the available experimental data for practical purposes. Once the model parameters in HF³D are fixed to the thermal neutron induced fission data, we extrapolate our calculation up to the threshold energy of the second chance fission. The energy dependence in FPY and isomeric ratio is thus calculated.

2. Modeling for Statistical decay of fission fragments

2.1. Generating fission fragment pairs

In the HF³D model, we apply the statistical Hauser-Feshbach theory to the fission fragment decay process, in which a competition between the neutron and γ -ray channels is properly included at all the compound decay stages. Instead of employing the MC technique to the Hauser-Feshbach theory^{18,19}, HF³D numerically integrates the emission probabilities over the distribution of fission fragment yield, as well as the distributions of excitation energy, spin and parity in each fragment. Although this deterministic method loses information on the correlated particle emission²³, it allows us to include a lot of fission fragment pairs that could have a tiny fission yield and never been sampled by the MC technique. This is particularly important for studying the production of radioactive isotopes¹⁷.

We assume that the fission fragment mass distribution $Y(A)$ is approximated by five Gaussians,

$$Y(A) = \sum_{i=1}^5 \frac{F_i}{\sqrt{2\pi}\sigma_i} \exp \left\{ -\frac{(A - A_m + \Delta_i)^2}{2\sigma_i^2} \right\}, \quad (1)$$

where σ_i and Δ_i are the Gaussian parameters, the index i runs from the low mass side, and the component of $i = 3$ is for the symmetric distribution ($\Delta_3 = 0$). $A_m = A_{\text{CN}}/2$ is the mid-point of the mass distribution, A_{CN} is the mass number of fissioning compound nucleus, and F_i is the fraction of each Gaussian component.

For the charge distribution $Z(A)$ we apply Wahl's Z_p model³³ with the parameters given in Ref¹¹. Combining the mass and charge distributions, we obtain the primary fission fragment distribution $Y(Z, A)$. Because the distribution is symmetric with respect to A_m ,

$$Y(Z_l, A_l) = Y(Z_{\text{CN}} - Z_l, A_{\text{CN}} - A_l) = Y(Z_h, A_h), \quad (2)$$

where l , h and CN denote the light, heavy fragment and compound nucleus, respectively. We abbreviate this by Y_k , where k stands for the k -th fission fragment pair of (Z_l, A_l) -

(Z_h, A_h) .

Setting the lowest mass number A_{\min} to 50, $A_{\max} = A_{\text{CN}} - A_{\min} = 186$ for the $n + {}^{235}\text{U}$ case, there will be more than 750 pairs of light and heavy fission fragments, namely more than 1,500 fission fragments. The energy conservation — the sum of the total excitation energy TXE and the total kinetic energy TKE cannot exceed the reaction Q -value — reduces the number of possible pairs. We fit a simple analytic function

$$\begin{aligned} \text{TKE}(A_h) &= (p_1 - p_2 A_h) \left\{ 1 - p_3 \exp\left(-\frac{(A_h - A_m)^2}{p_4}\right) \right\} \\ &+ \epsilon_{\text{TKE}} , \end{aligned} \quad (3)$$

to available experimental data of TKE at thermal energy, where $p_1 - p_4$ are the fitting parameters, and a small correction of ϵ_{TKE} ensures the average of Eq. (3) agrees with the evaluated $\overline{\text{TKE}}$. Since $\text{TKE}(A)$ is already averaged over the charge distribution $Z(A)$ for a fixed A number, we assume that the TKE of fragment pairs having the same A distributes according to their charge product $Z_l Z_h$, such that the average of different Z 's coincides with Eq. (3). TKE for a given (Z_l, A_l) - (Z_h, A_h) pair is denoted by $\text{TKE}(Z_l, A_l, Z_h, A_h)$, and TXE is calculated as

$$\begin{aligned} \text{TXE}(Z_l, A_l, Z_h, A_h) &= E_{\text{inc}} + B_n + [M_n(Z_{\text{CN}}, A_{\text{CN}}) - M_n(Z_l, A_l) - M_n(Z_h, A_h)]c^2 \\ &- \text{TKE}(Z_l, A_l, Z_h, A_h) , \end{aligned} \quad (4)$$

where E_{inc} is the incident neutron energy in the center-of-mass system, and B_n is the neutron binding energy of the target, and M_n represents the nuclear mass. When TXE becomes negative, we eliminate such pairs.

2.2. Hauser-Feshbach approach to the fission fragment decay

In the deterministic method, physical quantities that can be compared with experimental data are given by a fragment-yield weighted sum of the calculated results. For

example, the average number of prompt neutrons $\bar{\nu}$ is calculated as

$$\bar{\nu} = \sum_{k=1}^N Y_k \left(\bar{\nu}_l^{(k)} + \bar{\nu}_h^{(k)} \right), \quad (5)$$

where N is the total number of fragment pairs, and the neutron multiplicities $\bar{\nu}_{l,h}^{(k)}$ are given by integrating the neutron evaporation spectrum $\phi_{l,h}^{(k)}$ from the light or heavy fragment in the center-of-mass system,

$$\bar{\nu}_{l,h}^{(k)} = \int dE_x \sum_{J\Pi} \int d\epsilon R(J, \Pi) G(E_x) \phi_{l,h}^{(k)}(J, \Pi, E_x, \epsilon), \quad (6)$$

where $R(J, \Pi)$ is the probability of nucleus having the state of spin J and parity Π , and $G(E_x)$ is the distribution of excitation energy. They satisfy the normalization condition of $\sum_{J\Pi} R(J, \Pi) = 1$ and $\int G(E_x) dE_x = 1$.

For the spin and parity distributions we follow our previous work¹⁶, in which the spin-parity population distribution is expressed by

$$R(J, \Pi) = \frac{J + 1/2}{2f^2\sigma^2(U)} \exp \left\{ -\frac{(J + 1/2)^2}{2f^2\sigma^2(U)} \right\}, \quad (7)$$

where the parity distribution is just $1/2$, $\sigma^2(U)$ is the spin cut-off parameter, U is the excitation energy corrected by the pairing energy Δ as $U = E_x - \Delta$, and f is a scaling factor determined later by comparing the calculated results with experimental data.

We estimate the average excitation energies in each fragment, E_l and E_h , with the anisothermal model^{16,34,35} that is characterized by an anisothermal parameter R_T defined as the ratio of effective temperatures in the fission fragments

$$R_T = \frac{T_l}{T_h} = \sqrt{\frac{U_l a_h(U_h)}{U_h a_l(U_l)}}, \quad (8)$$

where $a(U)$ is the shell-effect corrected level density parameter at the excitation energy of U . In reality, TKE in Eq. (3) could have a distribution characterized by the width δ_{TKE} , which is empirically known to be about 8–10 MeV^{36,37}. This width propagates to the width of TXE through $\delta_{\text{TXE}} = \delta_{\text{TKE}}$, then perturbs the excitation energies of two fragments. Assuming Gaussian for the TXE distribution, each fragment has an excitation

energy distribution having the width of

$$\delta_{l,h} = \frac{\delta_{\text{TXE}}}{\sqrt{E_l^2 + E_h^2}} E_{l,h} , \quad (9)$$

hence

$$G(E_x) = \frac{1}{\sqrt{2\pi}\delta_{l,h}} \exp \left\{ -\frac{(E_x - E_{l,h})^2}{2\delta_{l,h}^2} \right\} . \quad (10)$$

By creating an initial population $P_0(E_x, J, \Pi) = R(J, \Pi)G(E_x)$ in a compound nucleus, the statistical Hauser-Feshbach calculation is performed from the highest excitation energy, with a variant version of the Hauser-Feshbach code CoH₃³⁸. We include the neutron and γ -ray channels only, since the charged particle emission is strongly suppressed in the neutron-rich nuclei. The neutron transmission coefficient is calculated by solving the Schrödinger equation for the spherical optical potential, where the global optical potential parameters of Koning and Delaroche³⁹ are adopted. The level densities in the continuum of fission fragments are calculated with the composite level density formulae of Gilbert and Cameron⁴⁰ with an updated parameterization⁴¹. At low excitation energies, the discrete level data are taken from the evaluated nuclear structure database RIPL-3⁴² (updated in 2012). The γ -ray transmission coefficient is calculated from the γ -ray strength functions. We adopt the generalized Lorentzian form of Kopecky and Uhl⁴³ for the E1 transition with the giant dipole resonance parameter systematics of Herman *et al.*⁴⁴. The higher multipolarities such as the M1 spin-flip mode and E2 take the standard Lorentzian form with the parameter systematics in RIPL-3⁴². In addition to the standard prescription of the γ -ray strength functions, we also consider the M1 scissors mode⁴⁵.

A probability of the number of emitted neutrons $P(\nu)$ can be determined by summing the ground and metastable state production probabilities of residuals, $P_{Z,A}(\nu)$, where Z, A are for the fission fragment, n is the number of emitted neutrons. Obviously $\sum_{\nu} P_{Z,A}(\nu) = 1$ because $P_0(E_x, J, \Pi)$ is normalized. For the k -th fragment pair of (Z_l, A_l) - (Z_h, A_h) , $P_{Z_l, A_l}(\nu)$ and $P_{Z_h, A_h}(\nu)$ are calculated separately, and the neutron multiplicity distribution

$P(\nu)$ is calculated by convoluting them;

$$P(\nu) = c \sum_{k=1}^N Y_k \sum_{i=0}^{\nu} P_{Z_l, A_l}(i) P_{Z_h, A_h}(\nu - i) , \quad (11)$$

where c is a normalization constant to satisfy $\sum_{\nu} P(\nu) = 1$. Equation (11) provides an alternative method to calculate $\bar{\nu}$, which reads

$$\bar{\nu} = \sum_{\nu} \nu P(\nu) . \quad (12)$$

3. Model Parameter Determination

3.1. Determination of the Gaussian parameters

We determine the five-Gaussian parameters Δ_i , σ_i , and F_i in Eq. (1) by fitting $Y(A)$ to the experimental data of Baba *et al.*³⁶, Hamsch³⁷, Pleasonton *et al.*⁴⁶, , Simon *et al.*⁴⁷, Straede *et al.*⁴⁸, and Zeynalov *et al.*⁴⁹ for the thermal neutron induced fission on ²³⁵U. These experimental data are reported as the primary fission fragment yield.

Since the mass distribution is symmetric with respect to A_m , relations like $\Delta_1 = -\Delta_5$, $\sigma_2 = \sigma_4$, hold. The normalization condition reads $2(F_1 + F_2) + F_3 = 2$. The obtained Gaussian parameters are $F_1 = 0.7846$, $\Delta_1 = 23.00$, $\sigma_1 = 4.828$, $F_2 = 0.2032$, $\Delta_2 = 15.63$, $\sigma_2 = 2.728$, $F_3 = 0.002916$, and $\sigma_3 = 8.6$. Figure 1 shows the comparison of the five-Gaussian represented $Y(A)$ with the experimental data.

[Figure 1 about here.]

To predict the independent fission product yields for the ²³⁵U(n,f) reaction in the fast energy range, we need to estimate energy variations of the model parameters such as TKE and $Y(A)$ as a function of neutron incident energy. Because the experimental data of $Y(A)$ above the thermal energy are very limited, we estimate the energy dependence of the five-Gaussian parameters solely from the data of D'yachenko *et al.*⁵⁰, anchoring the thermal point determined separately as aforementioned. The fitting is performed to the data up to the second chance fission threshold, so that there is no guarantee of extrapolation to the

outside region. The fitted Gaussian parameters, to which we assumed a linear dependence on the neutron incident energy E_n in MeV, are

$$\Delta_1 = -\Delta_5 = 23.00 - 0.2592E_n , \quad (13)$$

$$\Delta_2 = -\Delta_4 = 15.63 - 0.1996E_n , \quad (14)$$

$$\sigma_1 = \sigma_5 = 4.828 + 0.1667E_n , \quad (15)$$

while $\sigma_2 = \sigma_4$ and σ_3 are energy independent. The fractions of each Gaussian are given by

$$F_2 = F_4 = 0.2032 - 0.01565E_n , \quad (16)$$

$$F_3 = 0.003 + 0.004E_n , \quad (17)$$

$$F_1 = F_5 = 1 - F_2 - F_3/2 . \quad (18)$$

3.2. Determination of the TKE parameters

The parameters of $\text{TKE}(A)$ in Eq. (3) are obtained by fitting this function to the experimental data of Baba *et al.*³⁶, Hamsch³⁷, Simon *et al.*⁴⁷, Zeynalov *et al.*⁴⁹, and D'yachenko *et al.*⁵⁰ for the thermal neutron induced fission on ^{235}U . The values of fitting parameters are $p_1 = 335.3$ MeV, $p_2 = 1.174$ MeV, $p_3 = 0.1876$, and $p_4 = 69.08$. ϵ_{TKE} is slightly adjusted so that $\overline{\text{TKE}}$ is equal to the recommended value of 170.5 MeV⁵¹. The quality of data fitting is demonstrated in Fig. 2.

[Figure 2 about here.]

The energy dependence of $\overline{\text{TKE}}$ is estimated directly from experimental data. Madland⁵² estimated a linear relationship between the neutron incident energy and $\overline{\text{TKE}}$. We introduce an equation similar to Eq (3) in order to take into account a small non-linear tendency seen in the experimental data in the fast energy region^{53,54}, which reads

$$\overline{\text{TKE}}(E_n) = (q_1 - q_2E_n) \left\{ 1 - q_3 \exp\left(-\frac{E_n}{q_4}\right) \right\} . \quad (19)$$

By fitting Eq. (19) to the data of Duke⁵⁴, we obtained $q_1 = 171.2$ MeV, $q_2 = 0.1800$, $q_3 = 0.0043$, and $q_4 = 0.3230$ MeV. Figure 3 shows the comparison of this function with the experimental data of Meadows and Budtz-Jørgensen⁵⁵, and Duke⁵⁴. At higher energies the mass-dependence of TKE is assumed to be the same as Eq. (3).

[Figure 3 about here.]

3.3. Determination of the model parameters in the Hauser-Feshbach calculation

The scaling factor f in Eq. (7) and the anisothermal parameter R_T in Eq. (8) are the key ingredients that control the statistical decay of the fission fragments in the HF³D model. In our previous study¹⁶, we adopted $R_T = 1.3$ and $f = 3.0$, which were roughly estimated. We need to revisit these parameters, since some model inputs such as the Gaussian parameters were revised. These parameters should be determined such that the calculated quantities from the primary fission fragment generated with the five Gaussians are consistent with many fission observables, which provides higher confidence in the calculated $Y_I(Z, A)$.

We discretize the anisothermal parameter R_T and the scaling factor f within some parameter ranges that are physically sound, and study their impact on some fission observables, $\bar{\nu}$, $\bar{\nu}(A)$, $P(\nu)$, and $Y_I(A)$. Unfortunately the experimental data are too uncertain and prevent us to perform a least-squares fit. However, we were still able to estimate reasonable values for these parameters.

For the neutron emission multiplicity distribution $P(\nu)$, there are several experimental data⁵⁶⁻⁵⁹ available to compare with our calculation. We confirmed that R_T modestly exerts influence upon $P(\nu)$, while it has a visible sensitivity to the mass-dependent neutron multiplicities $\bar{\nu}(A)$. We also noticed that the evaluated $\bar{\nu}$ can be reproduced by adjusting the scaling factor f . When we increase the scaling factor f , the spin distribution $R(J, \Pi)$ of

Eq. (7) becomes wider, and the system will have more higher spin populations. Increase in the scaling factor f brings significant reduction in $\bar{\nu}$. The neutron emission is somewhat hindered due to a spin mismatch between the compound and daughter nuclei, and it results in an increase in the γ -ray emission. We estimated $f = 3.0$ by comparing the evaluated $\bar{\nu}$ in JENDL-4 of 2.42 at the thermal energy.

Figure 4 shows an example of calculated $P(\nu)$ by changing the scaling factor f while R_T is fixed to 1.2, comparing with the experimental data⁵⁶⁻⁵⁹. Based on this exercise together with the calculated value of $\bar{\nu}$, we adopted $f = 3.0$, which gives a relatively good agreement with the experimental data.

[Figure 4 about here.]

An impact of R_T on the mass-dependent average neutron multiplicity $\bar{\nu}(A)$ is shown in Fig. 5, where the cases of $R_T = 1.2, 1.3$ and 1.4 are shown. We have already revealed that the $Y(Z, A, TKE)$ is the most important input to reproduce the sawtooth structure of $\bar{\nu}(A)$ ⁶⁰. Small adjustment can be possible by varying R_T . The scaling factor f is fixed at 3.0 where the best fit of $\bar{\nu}$ can be reproduced. Despite our observation that R_T does not change the shape of $P(\nu)$, $\bar{\nu}(A)$ is notably affected by R_T . Generally speaking, increase in R_T gives a modest change in $\bar{\nu}$ and $P(\nu)$ at the thermal energy.

According to Eq. (8), more excitation energy is given to the light fragments when $R_T > 1$, and the number of neutrons emitted from the light fragment increases. We noticed that a value of $R_T = 1.2$ reproduces the experimental data most reasonably. The measurement of $\bar{\nu}(A)$ could be very difficult in the whole fission product mass range, since the yield can be extremely small in some mass regions, and it obliges the measurement severe statistics. Because the deterministic method mitigates such a difficult condition, we emphasize that our calculated result is not just an estimation but prediction supported by consistent descriptions of several observables simultaneously.

[Figure 5 about here.]

These parameters also change the calculated mass chain yield of the independent FPY, $Y_I(A)$. We carried out comparisons of $Y_I(A)$ with the ones in the evaluated libraries by varying the R_T and f parameters. A representative result for $Y_I(A)$ with the parameters $R_T = 1.0, 1.2$ and 1.4 (the scaling factors $f = 3.0$) is shown in Fig. 6. The mass distribution somehow extends outward with increasing R_T . Similar to the case of $\bar{\nu}(A)$, $R_T = 1.2$ provides a reasonable agreement with the evaluated data. Considering the arguments in this section, we conclude $R_T = 1.2$ and $f = 3.0$ to be the best set of the constants in this study.

Figure 6 also indicates that the Hauser-Feshbach calculation for the neutron evaporation process successfully reproduces the post-neutron mass distribution $Y_I(A)$. The pre-neutron distribution $Y(A)$ represented by the Gaussians is symmetric with respect to A_m , and the symmetry is broken after the prompt neutron emission. The evaluated mass distribution of independent FPY, such as those in ENDF/B-VI and JENDL/FPY-2011, exhibits some noticeable yield peaks at $A = 93, 96$, and 99 in the light fragment and $A = 133, 134$ and 138 in the heavy fragment. The origin of some of these peaks can be understood from $\bar{\nu}(A)$. For instance the peaks at $A = 133$ and 134 can be related to the doubly magic nucleus at $A = 132$ appeared as a sudden drop in $\bar{\nu}(A)$. Similarly other peaks are formed due to the excitation energy sorting mechanism and the difference in the neutron separation energies. Our calculation reproduces the peaks at $A = 93, 96$ and 134 .

[Figure 6 about here.]

4. Results and Discussion

4.1. Calculated independent fission product yield

We compare our calculated independent yield with a limited number of experimental data. This is because the present HF³D model is more or less the proof of concept to

demonstrate the feasibility of fully deterministic calculations for FPY. The calculated $Y_I(Z, A)$ for several fission products are compared with the experimental data of Rudstam *et al.*⁶¹ in Fig. 7. Although HF³D is not able to fit the data precisely, general tendency is well reproduced. The C/E-value (Calculated/Experimental) varies from 0.10 (¹¹⁶Ag) to 6.12 (⁷⁷Ga) and the average is 1.03 ± 0.81 . This is partly because Wahl's Z_p model works reasonably well. Note that the experimental $Y_I(Z, A)$ data are not the direct measurements but derived from the cumulative data⁶².

[Figure 7 about here.]

4.2. Energy dependent result

To confirm the estimated incident energy dependence in $Y(A)$ and $\overline{\text{TKE}}$ in the HF³D model, we compare $\bar{\nu}$ with the evaluated values at energies above thermal. $\bar{\nu}$ tells us information on an energy balance amongst the total fission energy, TKE, the kinetic energy of evaporated neutrons, and the emitted γ -rays. We assume that the anisothermal parameter $R_T = 1.2$ and the scaling factor $f = 3.0$ determined at the thermal energy do not change, at least up to the second chance fission threshold. The calculated $\bar{\nu}$ is shown in Fig. 8, which compares with the evaluated $\bar{\nu}$ in ENDF/B-VIII.0 and JENDL-4⁶³ together with experimental data taken from EXFOR database. Our calculated values are fairly consistent with these evaluations, although slightly deviate below 2 MeV. The deviations from the evaluated values at 1 MeV are 2.1% (JENDL-4) and 2.5% (ENDF/B-VIII.0), respectively.

[Figure 8 about here.]

The mass-dependent average neutron multiplicity $\bar{\nu}(A)$ in Fig. 5 increases as the incident neutron energy. The changes in $\bar{\nu}(A)$ at each A are roughly uniform hence we do not show a figure, except in the mass regions near $A_l = 100$ and $A_h = 150$ where the rise seems to be slightly larger. It is reported that an extra energy is always transferred to

the heavy fragments when the incident energy increases⁶⁴. The current model, however, predicts increases in $\bar{\nu}(A)$ from both the light and heavy fragments, because we assumed R_T is constant. If R_T decreases as the incident neutron energy increases, the change in $\bar{\nu}(A)$ would be more prominent in the heavy fragment side. At this moment we have no clear reason and strong evidence to explain the reduction in R_T . It is also noted that the the mass region around $A = 118$ generated mostly by the symmetric fission mode that is expressed by $R_T = 1.0$. Due to very low yields around $A = 118$, we ignored this effect.

The distribution of fission fragment yield evolves from the primary $Y(A)$ (pre-neutron) to the independent yield $Y_I(A)$ (post-neutron) distributions, which are connected by the prompt neutron emission calculated with the Hauser-Feshbach theory. Figure 9 shows the comparison of the mass distributions for the pre- and post-neutron emission at four energies, together with the independent mass yields in JENDL-FPY/2011 at the thermal and fast energies. Obviously the difference between the thermal and fast energies is modest, since their energies are close each other. As the energy increases, the post-neutron distribution shifts toward the low- A side. This shift is larger in the mass regions of 100 and 150.

[Figure 9 about here.]

4.3. Evaluation of Isomeric Ratio

Radiochemical determination of independent yield ratios of isomers of known spins for $^{235}\text{U}(\text{n},\text{f})$ has been conducted for some of major fission products, *e.g.* $^{128,130,132}\text{Sb}$, $^{131,133}\text{Te}$, $^{132,134,136}\text{I}$, ^{135}Xe and ^{138}Cs , and summarized by Naik *et al.*⁶⁵. The reported partial yields of ground and isomeric states were determined by the cumulative yield after correcting the precursor contributions. The isomeric ratio is defined as

$$\text{IR} = \frac{Y_m}{Y_m + Y_g}, \quad (20)$$

where Y_g and Y_m are the partial yield of ground and isomeric states in a specific nuclide. Because measurements of the isomeric ratios for all the fission products often encounter technical difficulties, theoretical predictions are essential for evaluating the nuclear data files. A model widely used for evaluating the isomeric ratio data was first proposed by Madland and England^{14,15}. In the Madland-England (ME) model the average angular momentum of the initial fission fragment is considered as a model parameter. The spin distribution of the fragments after prompt neutron emission is

$$P(J) = P_0(2J + 1) \exp \left[-\frac{(J + 1/2)^2}{\langle J^2 \rangle} \right], \quad (21)$$

where P_0 is the normalization constant, $J_{rms} \equiv \sqrt{\langle J^2 \rangle}$ characterizes the angular momentum of an initial fragment. As given in Eq. (21), the fission fragments are assumed to be formed with a density distribution $P(J)$ of the total angular momentum J , which is parameterized by J_{rms} . The parameter J_{rms} is assumed to be constant for all fission fragment masses in the neutron induced fission, whereas J_{rms} varies with incident neutron energy. The model adopted $J_{rms} = 7.5$ for the thermal neutron induced fission for all the fission fragments.

The model gives IR or the branching ratio (Y_m/Y_g) for eight different cases, whether the fission product mass number is even or odd, whether the spin difference between the metastable (J_m) and ground state (J_g) $|J_m - J_g|$ is even or odd, and whether J_m is greater or less than J_g . Since predicted isomeric ratio by this model depends on $J_{m/g}$ and A only, all the nuclides having the same $J_{m/g}$ and even/odd A will have the same isomeric ratio. For example, the ME model gives the same isomeric ratio of IR = 0.707 for both ^{133}Xe and ^{135}Xe , nevertheless the experimental data⁶⁶ indicate they differ. In addition, due to the inherent simplification in the model, the accuracy of the estimated branching ratio could be limited, particularly when J_m is very high compared to J_g , or there are other possible metastable states. When a nuclide has more than one metastable state, the definition of IR must be corrected as $Y_m^{(i)}/(Y_g + \sum_k Y_m^{(k)})$.

We performed the HF³D model calculation for many primary fission fragments, and searched for all the levels in RIPL-3⁴² whose half-life is longer than 1 ms. This definition could be somewhat shorter than the half-life of commonly known metastable states. We paid special attention to include some high-lying metastable states. If its excitation energy is higher than the known level up to which RIPL-3 says there is no missing level, we postulates several levels between these states according to the CoH₃ level density and spin-parity distributions to fill the gap. Figure 10 shows the ratio of calculated IRs with the ME model (JENDL/FPY-2011) to those with HF³D, plotted against Z^2/A . The mean value of the ratio 2.75 ± 4.90 indicates a clear disagreement between the ME and HF³D models, and the ME model tends to overestimate IR.

[Figure 10 about here.]

The disagreement is also evident in Figure 11, where IRs for each individual independent fission product, whose yield is more than 10^{-4} , are shown. The upper panel shows the calculated fractional independent yields for the ground and metastable states, and the lower panel shows their IRs together with some experimental IRs^{65,67}. Although the experimental IR data are scarce, we can compare some of the results for ⁹⁰Rb, ¹³¹Sn, ^{128,130,132}Sb, ^{131,133}Te, ^{132,134,136}I, ^{133,135}Xe and ¹³⁸Cs.

[Figure 11 about here.]

One of the interesting features in our model is that we find two isomeric states in ¹³¹Te. The experimental IR was reported in 1995 and the second metastable state with $J^\pi = (23/2)^+$ was reported in 1998⁶⁸, and both ENDF/B-VII and JENDL/FPY-2011 only include the first metastable state so far. This means the reported IR is understood to be $(Y_{m1} + Y_{m2})/(Y_g + Y_{m1} + Y_{m2})$, while we calculated this as $Y_{m1}/(Y_g + Y_{m1} + Y_{m2})$ and $Y_{m2}/(Y_g + Y_{m1} + Y_{m2})$ independently. This is why our calculation looks lower than the experimental data. In fact our calculated $(Y_{m1} + Y_{m2})/(Y_g + Y_{m1} + Y_{m2})$ value agrees fairly well with the experimental data.

Besides ^{134}I and ^{136}I , the ME model better agrees with the experimental data than our model. We examined if some even/odd effects in the spin and mass number reveal systematic features in the ME prediction. However no prominent rule was found.

In the case of $^{128,130}\text{Sb}$, where J_g is higher than J_m , our model predicts IR pretty reasonably. That said, our calculation misses the experimental data of ^{136}I , where the difference in J_g and J_m is relatively large. At this moment we have no simple explanation of why our prediction fails in some cases, although there are not so many. Missing high spin levels in the RIPL data file can cause such discrepancies and thus it requires the better nuclear structure data.

The energy dependence of IR for is confirmed. It is revealed that IR is insensitive to the incident neutron energy in general. In Figure 12, ^{100}Y and ^{138}Cs are chosen as examples. While the fractional independent yield of ground and metastable states change slightly as the incident neutron energy increases, the IRs remain constant.

[Figure 12 about here.]

5. Conclusion

We developed a new method to calculate the independent fission product yield $Y_I(Z, A)$ and the isomeric ratio IR by applying the statistical Hauser-Feshbach theory to the decay process of the primary fission fragment pairs for $^{235}\text{U}(n_{\text{th}}, f)$, where about 1,000 nuclides are involved. Instead of employing the Monte Carlo sampling technique that was commonly used in the past, our model, called HF³D, is based on the fully deterministic technique. The input data, *e.g.* the mass distribution of the primary fission fragment and the fragment kinetic energy were determined by fitting analytical functions to the available experimental data, the charge distribution was generated by the Z_p model, and the incident neutron energy dependence was also determined according to the experimental data. Besides these inputs, we adjusted the scale factor f in the spin distribution and the

anisothermal parameter R_T , which define the initial configuration of the fission fragments, to reproduce some observables in fission, such as the average prompt neutron multiplicity $\bar{\nu}$, its mass dependence $\bar{\nu}(A)$, and the neutron emission multiplicity distribution $P(\nu)$.

Beginning with the initial configuration characterized by the primary fission fragment pair, the total kinetic energy, the excitation energy, and the initial spin and parity distributions, we calculated the neutron evaporation both from the light and heavy fragments of $^{235}\text{U}(\text{n},\text{f})$. We demonstrated that the anisothermal parameter R_T is sensitive to $\bar{\nu}(A)$, while the initial distribution controlled by the scale factor f impacts on $P(\nu)$. Once these parameters were tuned, we showed that the calculated post-neutron mass distribution $Y_I(A)$ agreed well with that in JENDL/FPY-2011.

We demonstrated that the symmetric mass distribution of the primary fission fragment $Y(A)$ with respect to $A_m = 236/2 = 118$ is broken due to the prompt neutron emission, and the resulting $Y_I(A)$ evidently shows the mass peaks at $A = 93, 96$ and 134 seen also in the evaluated FPY data.

In addition to $Y_I(Z, A)$, the model also provides the IR for the nuclides having any short-lived or long-lived isomeric states. We observed that IRs predicted by the Madland-England model^{14,15} tend to be larger than our calculation.

Optimizing our model input parameters on the thermal neutron data, we extrapolated the model calculations up to 5 MeV, where only the first chance fission takes place. Generally speaking IRs are insensitive to the incident neutron energy.

As a final remark, by connecting the HF³D method with the decay data library, we will be able to predict the cumulative fission product yield as well as the mass chain yield, for which abundant experimental data are accessible. This would be a powerful tool to evaluate the independent and cumulative fission product yield data simultaneously and consistently in the energy-dependent manner, and obviously be our next stride.

6. Acknowledgements

We are grateful to T. Yoshida of Tokyo Institute of Technology (Tokyo Tech.) and K. Nishio of Japan Atomic Energy Agency (JAEA) for valuable discussions. This work was partially supported by the grant “Development of prompt-neutron measurement in fission by surrogate reaction method and evaluation of neutron-energy spectra,” entrusted to JAEA by Ministry of Education, Culture, Sports, Science and Technology. This work was partly carried out under the auspices of the National Nuclear Security Administration of the U.S. Department of Energy at Los Alamos National Laboratory under Contract No. DE-AC52-06NA25396. One of the authors (TK) would like to thank the WRHI (World Research Hub Initiative) program at Tokyo Tech. for supporting this work.

References

- [1] England TR, Rider BF. Evaluation and compilation of fission product yields. Los Alamos National Laboratory; 1994. ENDF-349, LA-UR-94-3106.
- [2] Yoshida T, Nakasima R. Decay Heat Calculations Based on Theoretical Estimation of Average Beta- and Gamma-Energies Released from Short-Lived Fission Products. *Journal of Nuclear Science and Technology*. 1981;18(6):393 – 407. Available from: <https://doi.org/10.1080/18811248.1981.9733273>.
- [3] Yoshida T, Wakasugi Y, Hagura N. Pandemonium Problem in Fission-Product Decay Heat Calculations Revisited. *Journal of Nuclear Science and Technology*. 2008;45(8):713 – 717. Available from: <http://www.tandfonline.com/doi/abs/10.1080/18811248.2008.9711471>.
- [4] Chiba G. Consistent adjustment of radioactive decay and fission yields data with measurement data of decay heat and β -delayed neutron activities. *Annals of Nuclear Energy*. 2017;101(Supplement C):23 – 30. Available from: <http://www.sciencedirect.com/science/article/pii/S0306454916305849>.
- [5] Yoshida T, Okajima S, Sakurai T, Nakajima K, Yamane T, Katakura Ji, et al. Evaluation of Delayed

- Neutron Data for JENDL-3.3. *Journal of Nuclear Science and Technology*. 2002;39(sup2):136 – 139. Available from: <https://doi.org/10.1080/00223131.2002.10875059>.
- [6] Chiba G, Tsuji M, Narabayashi T. Sensitivity and uncertainty analysis for reactor stable period induced by positive reactivity using one-point adjoint kinetics equation. *Journal of Nuclear Science and Technology*. 2013;50(12):1150 – 1160. Available from: <https://doi.org/10.1080/00223131.2013.838332>.
- [7] Hayes AC, Friar JL, Garvey GT, Ibeling D, Jungman G, Kawano T, et al. Possible origins and implications of the shoulder in reactor neutrino spectra. *Phys Rev D*. 2015 Aug;92:033015. Available from: <http://link.aps.org/doi/10.1103/PhysRevD.92.033015>.
- [8] Shibagaki S, Kajino T, J MG, Chiba S, Nishimura S, Lorusso G. Relative Contributions of the Weak, Main, and Fission-recycling r-process. *The Astrophysical Journal*. 2016;816(2):79. Available from: <http://stacks.iop.org/0004-637X/816/i=2/a=79>.
- [9] Chadwick MB, Kawano T, Barr DW, Mac Innes MR, Kahler AC, T G, et al. Fission Product Yields from Fission Spectrum $n+^{239}\text{Pu}$ for ENDF/B-VII.1. *Nuclear Data Sheets*. 2010;111(12):2923 – 2964. Available from: <http://www.sciencedirect.com/science/article/pii/S009037521000102X>.
- [10] Kawano T, Chadwick MB. Estimation of ^{239}Pu independent and cumulative fission product yields from the chain yield data using a Bayesian technique. *Journal of Nuclear Science and Technology*. 2013;50(10):1034 – 1042. Available from: <https://doi.org/10.1080/00223131.2013.830580>.
- [11] Wahl AC. Systematics of Fission-Product Yields. Los Alamos National Laboratory; 2002. LA-13928.
- [12] Katakura J. JENDL FP Decay Data File 2011 and Fission Yields Data File 2011. Japan Atomic Energy Agency; 2012. JAEA-Data/Code 2011-025.
- [13] Katakura J, Minato K, Ohgama F. Revision of the JENDL FP Fission Yield Data. *EPJ Web of Conferences*. 2016;111:08004-1 – 5. Available from: https://www.epj-conferences.org/articles/epjconf/abs/2016/06/epjconf_wonder2016_08004/epjconf_wonder2016_08004.html.
- [14] Madland DG, England TR. The Influence of Isomeric States on Independent Fission Product Yields. *Nuclear Science and Engineering*. 1977;64:859 – 865. Available from: <https://doi.org/10.13182/>

NSE77-A14501.

- [15] Madland DG, England TR. Distribution of independent fission-product yields to isomeric states. Los Alamos National Laboratory; 1994. LA-6595-MS.
- [16] Kawano T, Talou P, Stetcu I, Chadwick MB. Statistical and evaporation models for the neutron emission energy spectrum in the center-of-mass system from fission fragments. Nuclear Physics A. 2013;913(2):51 – 70. Available from: <http://www.sciencedirect.com/science/article/pii/S0375947413005952>.
- [17] Stetcu I, Talou P, Kawano T, Jandel M. Isomer production ratios and the angular momentum distribution of fission fragments. Phys Rev C. 2013 Oct;88:044603. Available from: <http://link.aps.org/doi/10.1103/PhysRevC.88.044603>.
- [18] Becker B, Talou P, Kawano T, Danon Y, Stetcu I. Monte Carlo Hauser-Feshbach predictions of prompt fission γ rays: Application to $n_{\text{th}} + {}^{235}\text{U}$, $n_{\text{th}} + {}^{239}\text{Pu}$, and ${}^{252}\text{Cf}$ (sf). Phys Rev C. 2013 Jan;87:014617. Available from: <http://link.aps.org/doi/10.1103/PhysRevC.87.014617>.
- [19] Litaize O, Serot O. Investigation of phenomenological models for the Monte Carlo simulation of the prompt fission neutron and γ emission. Phys Rev C. 2010 Nov;82:054616. Available from: <https://link.aps.org/doi/10.1103/PhysRevC.82.054616>.
- [20] Randrup J, Vogt R. Calculation of fission observables through event-by-event simulation. Phys Rev C. 2009 Aug;80:024601. Available from: <https://link.aps.org/doi/10.1103/PhysRevC.80.024601>.
- [21] Randrup J, Vogt R. Refined treatment of angular momentum in the event-by-event fission model freya. Phys Rev C. 2014 Apr;89:044601. Available from: <https://link.aps.org/doi/10.1103/PhysRevC.89.044601>.
- [22] Schmidt KH, Jurado B, Amouroux C, Schmitt C. General Description of Fission Observables: GEF Model Code. Nuclear Data Sheets. 2016;131:107 – 221. Special Issue on Nuclear Reaction Data. Available from: <http://www.sciencedirect.com/science/article/pii/S0090375215000745>.
- [23] Talou P, Vogt R, Randrup J, Rising ME, Pozzi SA, Nakae L, et al. Correlated Prompt Fission Data in Transport Simulations. European Physical Journal. 2017;.

- [24] Aritomo Y, Chiba S. Fission process of nuclei at low excitation energies with a Langevin approach. Phys Rev C. 2013 Oct;88:044614. Available from: <https://link.aps.org/doi/10.1103/PhysRevC.88.044614>.
- [25] Aritomo Y, Chiba S, Ivanyuk F. Fission dynamics at low excitation energy. Phys Rev C. 2014 Nov;90:054609. Available from: <https://link.aps.org/doi/10.1103/PhysRevC.90.054609>.
- [26] Usang MD, Ivanyuk FA, Ishizuka C, Chiba S. Effects of microscopic transport coefficients on fission observables calculated by the Langevin equation. Phys Rev C. 2016;94:044602. Available from: <https://link.aps.org/doi/10.1103/PhysRevC.94.044602>.
- [27] Ishizuka C, Usang MD, Ivanyuk FA, Maruhn JA, Nishio K, Chiba S. Four-dimensional Langevin approach to low-energy nuclear fission of ^{236}U . Phys Rev C. 2017;96:064616. Available from: <https://link.aps.org/doi/10.1103/PhysRevC.96.064616>.
- [28] Usang MD, Ivanyuk FA, Ishizuka C, Chiba S. Analysis of the total kinetic energy of fission fragments with the Langevin equation. Phys Rev C. 2017;96:064617. Available from: <https://link.aps.org/doi/10.1103/PhysRevC.96.064617>.
- [29] Sierk AJ. Langevin model of low-energy fission. Phys Rev C. 2017 Sep;96:034603. Available from: <https://link.aps.org/doi/10.1103/PhysRevC.96.034603>.
- [30] Randrup J, Möller P, Sierk AJ. Fission-fragment mass distributions from strongly damped shape evolution. Phys Rev C. 2011 Sep;84:034613. Available from: <https://link.aps.org/doi/10.1103/PhysRevC.84.034613>.
- [31] Randrup J, Möller P. Brownian Shape Motion on Five-Dimensional Potential-Energy Surfaces:Nuclear Fission-Fragment Mass Distributions. Phys Rev Lett. 2011 Mar;106:132503. Available from: <https://link.aps.org/doi/10.1103/PhysRevLett.106.132503>.
- [32] Möller P, Randrup J. Calculated fission-fragment yield systematics in the region $74 \leq Z \leq 94$ and $90 \leq N \leq 150$. Phys Rev C. 2015 Apr;91:044316. Available from: <https://link.aps.org/doi/10.1103/PhysRevC.91.044316>.
- [33] Wahl AC. Nuclear-charge distribution and delayed-neutron yields for thermal-neutron-induced fission

- of ^{235}U , ^{233}U , and ^{239}Pu and for spontaneous fission of ^{252}Cf . Atomic Data and Nuclear Data Tables. 1988;39(1):1 – 156. Available from: <http://www.sciencedirect.com/science/article/pii/0092640X88900162>.
- [34] Ohsawa T, Horiguchi T, Hayashi H. Multimodal analysis of prompt neutron spectra for $^{237}\text{Np}(n,f)$. Nuclear Physics A. 1999;653(1):17 – 26. Available from: <http://www.sciencedirect.com/science/article/pii/S0375947499001566>.
- [35] Ohsawa T, Horiguchi T, Mitsuhashi M. Multimodal analysis of prompt neutron spectra for $^{238}\text{Pu}(sf)$, $^{240}\text{Pu}(sf)$, $^{242}\text{Pu}(sf)$ and $^{239}\text{Pu}(n_{th},f)$. Nuclear Physics A. 2000;665(1):3 – 12. Available from: <http://www.sciencedirect.com/science/article/pii/S0375947499006867>.
- [36] Baba H, Saito T, Takahashi N, Yokoyama A, Miyauchi T, Mori S, et al. Role of Effective Distance in the Fission Mechanism Study by the Double-energy Measurement for Uranium Isotopes. Journal of Nuclear Science and Technology. 1997;34(9):871 – 881. Available from: <https://doi.org/10.1080/18811248.1997.9733759>.
- [37] Hamsch FJ. (personal communication);
- [38] Kawano T, Talou P, Chadwick MB, Watanabe T. Monte Carlo Simulation for Particle and γ -Ray Emissions in Statistical Hauser-Feshbach Model. Journal of Nuclear Science and Technology. 2010 May;47(5):462 – 469. Available from: <http://www.tandfonline.com/doi/abs/10.1080/18811248.2010.9711637>.
- [39] Koning AJ, Delaroche JP. Local and global nucleon optical models from 1 keV to 200 MeV. Nuclear Physics A. 2003;713(3):231 – 310. Available from: <http://www.sciencedirect.com/science/article/pii/S0375947402013210>.
- [40] Gilbert A, Cameron AGW. A composite nuclear-level density formula with shell corrections. Can J Phys. 1965;43. Available from: <http://www.nrcresearchpress.com/doi/abs/10.1139/p65-139#.V6IU247raQ8>.
- [41] Kawano T, Chiba S, Koura H. Phenomenological Nuclear Level Densities using the KTUY05 Nuclear Mass Formula for Applications Off-Stability. Journal of Nuclear Science and Technology. 2006;43(1):1

- 8. Available from: <http://www.tandfonline.com/doi/abs/10.1080/18811248.2006.9711062>.
- [42] Capote R, Herman M, Obložinský P, Young PG, Goriely S, Belgia T, et al. RIPL - Reference Input Parameter Library for Calculation of Nuclear Reactions and Nuclear Data Evaluations. Nuclear Data Sheets. 2009;110(12):3107 – 3214. Available from: <http://www.sciencedirect.com/science/article/pii/S0090375209000994>.
- [43] Kopecky J, Uhl M. Test of gamma-ray strength functions in nuclear reaction model calculations. Phys Rev C. 1990 May;41:1941 – 1955. Available from: <http://link.aps.org/doi/10.1103/PhysRevC.41.1941>.
- [44] Herman M, Capote R, Sin M, Trkov A, Carlson BV, Obložinský P, et al. EMPIRE-3.2 Malta, Modular system for nuclear reaction calculations and nuclear data evaluation User's Manual. International Atomic Energy Agency; 2013. INDC(NDS)-0603.
- [45] Mumpower MR, Kawano T, Ullmann JL, Krtička M, Sprouse TM. Estimation of $M1$ scissors mode strength for deformed nuclei in the medium- to heavy-mass region by statistical Hauser-Feshbach model calculations. Phys Rev C. 2017 Aug;96:024612. Available from: <https://link.aps.org/doi/10.1103/PhysRevC.96.024612>.
- [46] Pleasonton F, Ferguson RL, Schmitt HW. Prompt Gamma Rays Emitted in the Thermal-Neutron-Induced Fission of ^{235}U . Phys Rev C. 1972 Sep;6:1023 – 1039. Available from: <https://link.aps.org/doi/10.1103/PhysRevC.6.1023>.
- [47] Simon G, Trochon J, Brisard F, Signarbieux C. Pulse height defect in an ionization chamber investigated by cold fission measurements. Nuclear Instruments and Methods in Physics Research Section A: Accelerators, Spectrometers, Detectors and Associated Equipment. 1990;286(1):220 – 229. Available from: <http://www.sciencedirect.com/science/article/pii/016890029090224T>.
- [48] Straede C, Budtz-Jørgensen C, Knitter HH. $^{235}\text{U}(n,f)$ Fragment mass-, kinetic energy- and angular distributions for incident neutron energies between thermal and 6 MeV. Nuclear Physics A. 1987;462(1):85 – 108. Available from: <http://www.sciencedirect.com/science/article/pii/0375947487903812>.

- [49] Zeynalov S, Furman W, Hamsch FJ. Investigation of mass-TKE distributions of fission fragments from the U-235(n,f)- reaction in resonances. ISINN-13. 2006; Available from: <http://isinn.jinr.ru/proceedings/isinn-13/pdf/351.pdf>.
- [50] D'yachenko PP, Kuzminov BD, Tarasko MZ. Energy and mass distribution of fragments from fission of U-235 by monoenergetic neutrons from 0. to 15.5 MeV. Soviet Journal of Nuclear Physics. 1969;8.
- [51] Wagemans C. The Nuclear Fission Process. CRC Press; 1991.
- [52] Madland DG. Total prompt energy release in the neutron-induced fission of ^{235}U , ^{238}U , and ^{239}Pu . Nuclear Physics A. 2006;772(3):113 – 137. Available from: <http://www.sciencedirect.com/science/article/pii/S0375947406001503>.
- [53] Lestone JP, Strother TT. Energy Dependence of Plutonium and Uranium Average Fragment Total Kinetic Energies. Nuclear Data Sheets. 2014;118(Supplement C):208 – 210. Available from: <http://www.sciencedirect.com/science/article/pii/S0090375214000684>.
- [54] Duke D. Fission fragment mass distributions and total kinetic energy release of ^{235}U -uranium and ^{238}U -uranium in neutron-induced fission at intermediate and fast neutron energies. 2014; Ph.D Thesis, Colorado State University.
- [55] Meadows JW, Budtz-Jørgensen C. The fission fragment angular distributions and total kinetic energies for ^{235}U (n,f) from .18 to 8.83 MeV. Argonne National Laboratory; 1982. ANL/NDM-64.
- [56] J W Boldeman AWD. Prompt nubar measurements for thermal neutron fission. AAEC-E. 1967;172. Available from: <https://trove.nla.gov.au/work/35052889>.
- [57] Franklyn CB, Hofmeyer C, Mingay DW. Angular correlation of neutrons from thermal-neutron fission of ^{235}U . Physics Letters B. 1978;78(5):564 – 567. Available from: <http://www.sciencedirect.com/science/article/pii/0370269378906408>.
- [58] Diven BC, Martin HC, Taschek RF, Terrell J. Multiplicities of Fission Neutrons. Phys Rev. 1956 Feb;101:1012 – 1015. Available from: <https://link.aps.org/doi/10.1103/PhysRev.101.1012>.
- [59] Holden NE, Zucker MS. Prompt Neutron Emission Multiplicity Distribution and Average Values (Nubar) at 2200 m/s for the Fissile Nuclides. Nuclear Science and Engineering. 1988;98(2):174 –

181. Available from: <https://doi.org/10.13182/NSE88-A28498>.
- [60] Talou P, Becker B, Kawano T, Chadwick MB, Danon Y. Advanced Monte Carlo modeling of prompt fission neutrons for thermal and fast neutron-induced fission reactions on ^{239}Pu . *Phys Rev C*. 2011 Jun;83:064612. Available from: <http://link.aps.org/doi/10.1103/PhysRevC.83.064612>.
- [61] Rudstam G, Aagaard P, Ekström B, Lund E, Göktürk H, Zwicky HU. Yields of Products from Thermal Neutron-Induced Fission of ^{235}U . *Radiochimica Acta*. 1990;49(4):155 – 192.
- [62] Rudstam G. The determination of nuclear reaction yields by means of an isotope-separator-on-line (ISOL) system. *Nuclear Instruments and Methods in Physics Research Section A: Accelerators, Spectrometers, Detectors and Associated Equipment*. 1987;256(3):465 – 483. Available from: <http://www.sciencedirect.com/science/article/pii/0168900287902907>.
- [63] Shibata K, Iwamoto O, Nakagawa T, Iwamoto N, Ichihara A, Kunieda S, et al. JENDL-4.0: A New Library for Nuclear Science and Engineering. *J Nucl Sci Technol*. 2011 Jan;48:1 – 30. Available from: <http://www.tandfonline.com/doi/abs/10.1080/18811248.2011.9711675>.
- [64] Müller R, Naqvi AA, Käppeler F, Dickmann F. Fragment velocities, energies, and masses from fast neutron induced fission of ^{235}U . *Phys Rev C*. 1984 Mar;29:885 – 905. Available from: <https://link.aps.org/doi/10.1103/PhysRevC.29.885>.
- [65] Naik H, Dange SP, Singh RJ, Datta T. Systematics of fragment angular momentum in low-energy fission of actinides. *Nuclear Physics A*. 1995;587(2):273 – 290. Available from: <http://www.sciencedirect.com/science/article/pii/0375947494008214>.
- [66] Ford GP, Wolfsberg K, Erdal BR. Independent yields of the isomers of ^{133}Xe and ^{135}Xe for neutron-induced fission of ^{233}U , ^{235}U , ^{238}U , and $^{242}\text{Am}^m$. *Phys Rev C*. 1984 Jul;30:195–213. Available from: <https://link.aps.org/doi/10.1103/PhysRevC.30.195>.
- [67] Reeder PL, Warner RA, Ford GP, Willmes H. Independent isomer yield ratio of ^{90}Rb from thermal neutron fission of ^{235}U . *Phys Rev C*. 1985 Oct;32:1327–1334. Available from: <https://link.aps.org/doi/10.1103/PhysRevC.32.1327>.
- [68] Fogelberg B, Mach H, Gausemel H, Omtvedt JP, Mezilev KA. New High Spin Isomers Ob-

tained in Thermal Fission. AIP Conference Proceedings. 1998;447:191. Available from: <http://aip.scitation.org/doi/abs/10.1063/1.56702>.

Figure Captions

Figure 1 The experimental primary fission fragment yield distribution $Y(A)$ and the resulting function of Eq. (1).

Figure 2 The total kinetic energy, TKE, as a function of the heavy fragment mass number. The solid line is Eq. (3) with the parameters given in the text.

Figure 3 The total kinetic energy, TKE, as a function of incident neutron energy. The solid line is Eq. (19), and the dashed line is obtained by Madland⁵². Meadows⁵⁵ data are adjusted to $\overline{\text{TKE}}(E_{\text{th}}) = 170.5$ MeV.

Figure 4 The calculated $P(\nu)$ with the anisothermal parameter $R_T = 1.2$ and the scaling factor $f = 2.0, 2.5$ and 3.0 .

Figure 5 The calculated $\bar{\nu}(A)$ with the scaling factors $f = 3.0$ and the anisothermal parameter $R_T = 1.2, 1.3$ and 1.4 .

Figure 6 The calculated post-neutron distribution of fission products $Y_I(A)$ with the scaling factor $f = 3.0$ and the anisothermal parameter $R_T = 1.0, 1.2$ and 1.4 .

Figure 7 Comparison of the calculated independent yield $Y_I(Z, A)$ with the experimental data reported by Rudstam *et al.*⁶¹

Figure 8 The calculated average number of prompt neutrons $\bar{\nu}$ comparing with the evaluated $\bar{\nu}$ in ENDF/B-VIII (dashed line) and JENDL-4 (dotted line), and experimental data taken from the EXFOR databaes.

Figure 9 The calculated $Y_I(A)$ at (a) thermal, (b) fast energy, (c) 3, and (d) 5 MeV. The evaluated $Y_I(A)$ in JENDL/FPY-2011 at the thermal and fast energies are also depicted in the top panels.

Figure 10 The ratio of the Madland-England model to the Hauser-Feshbach calculation by HF³D for all possible fission products containing the metastable state.

Figure 11 Calculated fractional independent yields (upper panel) and IRs (bottom panel) for the nuclides that have the ground state yield of greater than 1×10^{-4} . The IRs are shown together with JENDL/FPY-2011 data compiled by the Madland-England model, and some experimental data. The first and the second isomeric states are denoted by the subscript.

Figure 12 Energy dependence of ground and metastable state yield (top frame) and isomeric ratio (bottom frame) of ^{100}Y and ^{138}Cs .

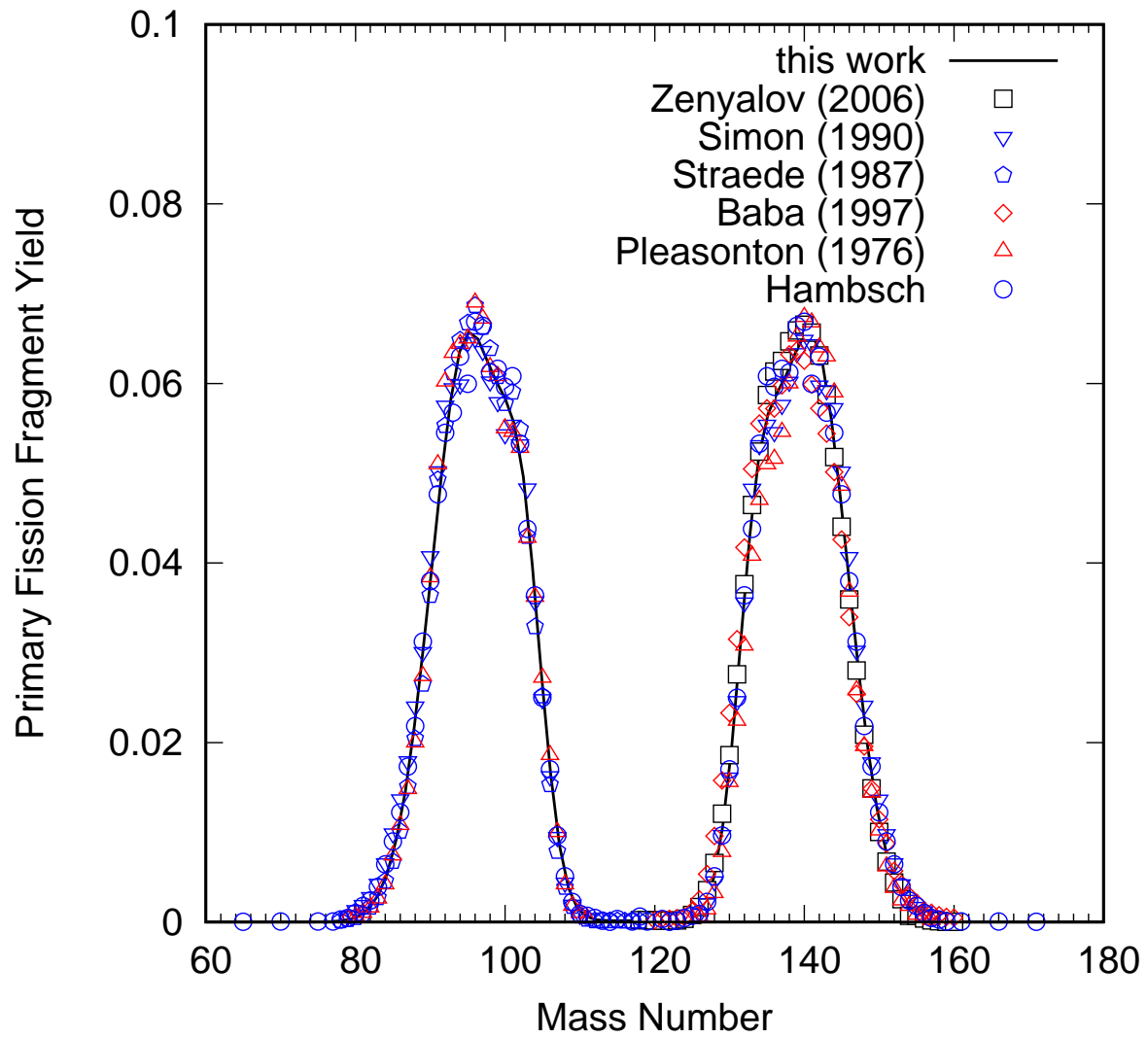


Figure 1 The experimental primary fission fragment yield distribution $Y(A)$ and the resulting function of Eq. (1).

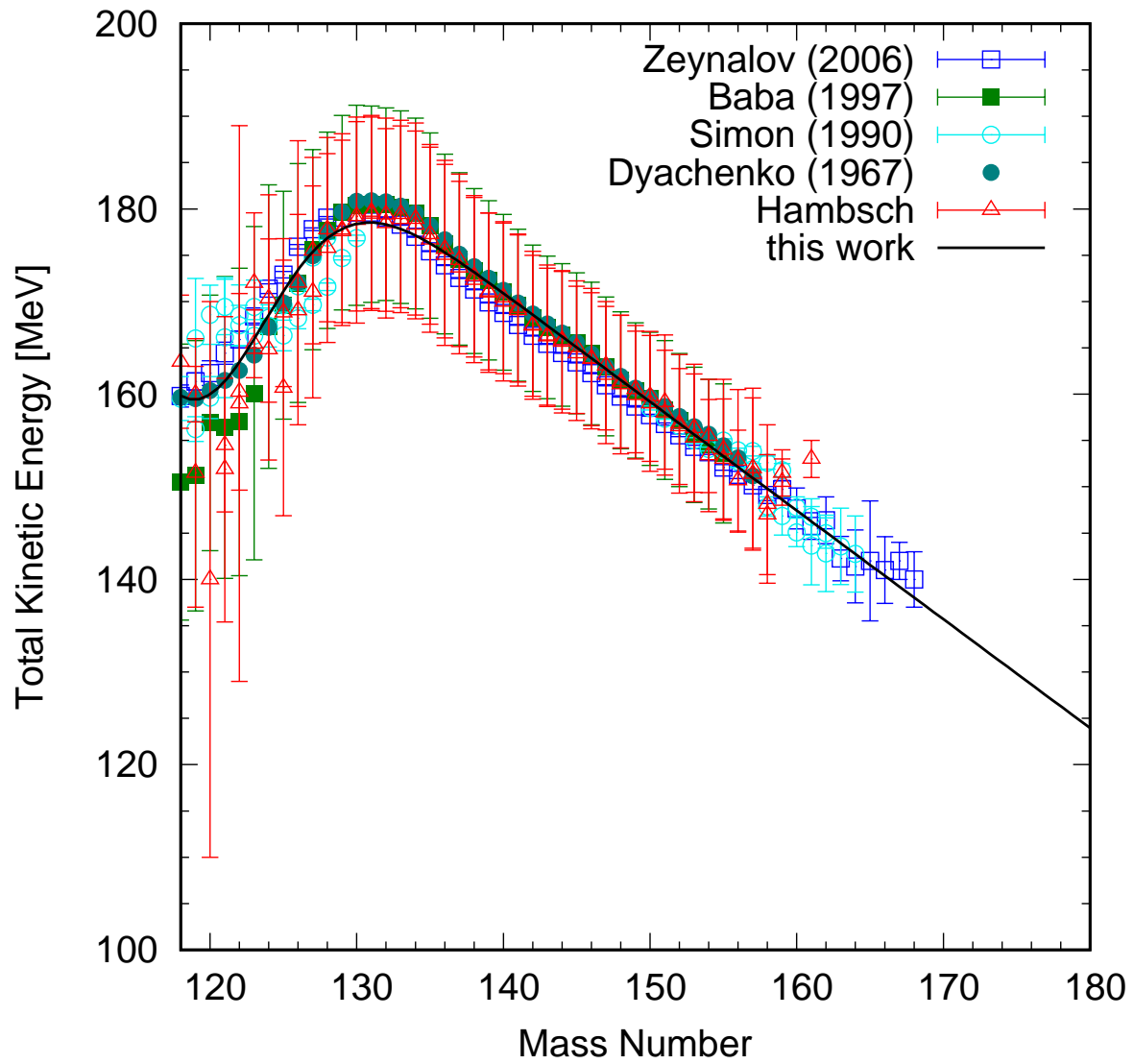


Figure 2 The total kinetic energy, TKE, as a function of the heavy fragment mass number. The solid line is Eq. (3) with the parameters given in the text.

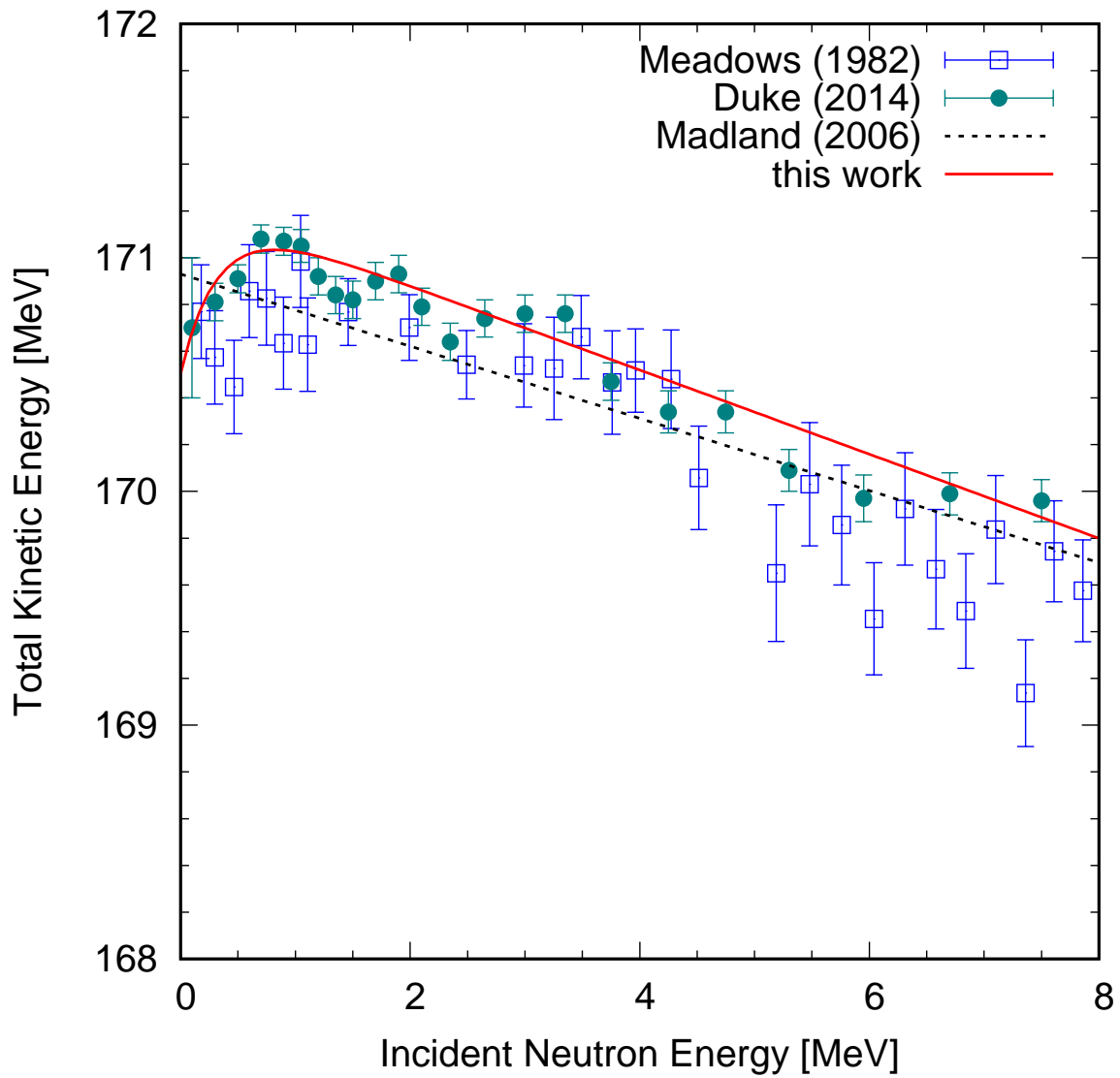


Figure 3 The total kinetic energy, TKE, as a function of incident neutron energy. The solid line is Eq. (19), and the dashed line is obtained by Madland⁵². Meadows⁵⁵ data are adjusted to $\overline{\text{TKE}}(E_{\text{th}}) = 170.5$ MeV.

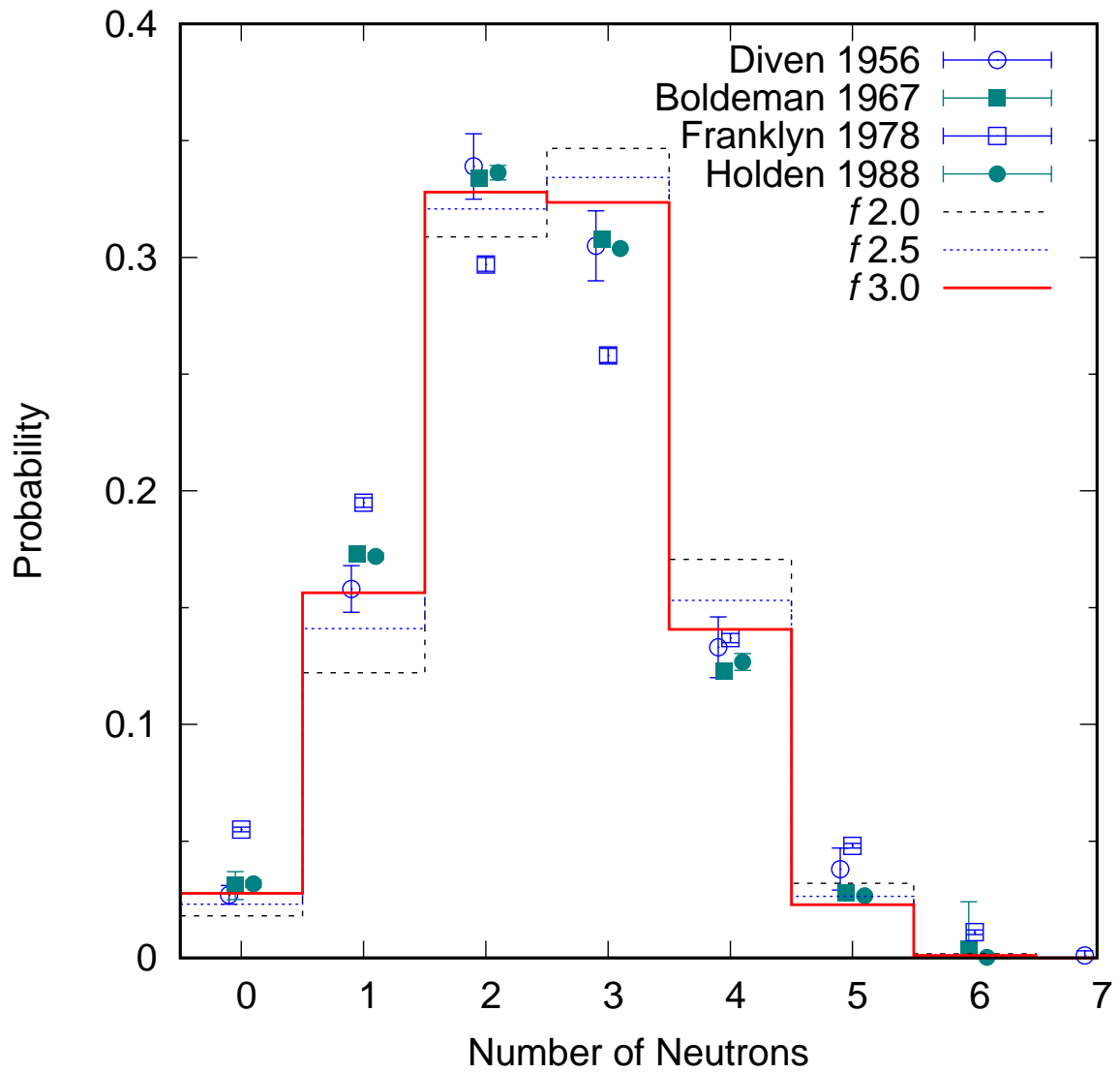


Figure 4 The calculated $P(\nu)$ with the anisothermal parameter $R_T = 1.2$ and the scaling factor $f = 2.0$, 2.5 and 3.0.

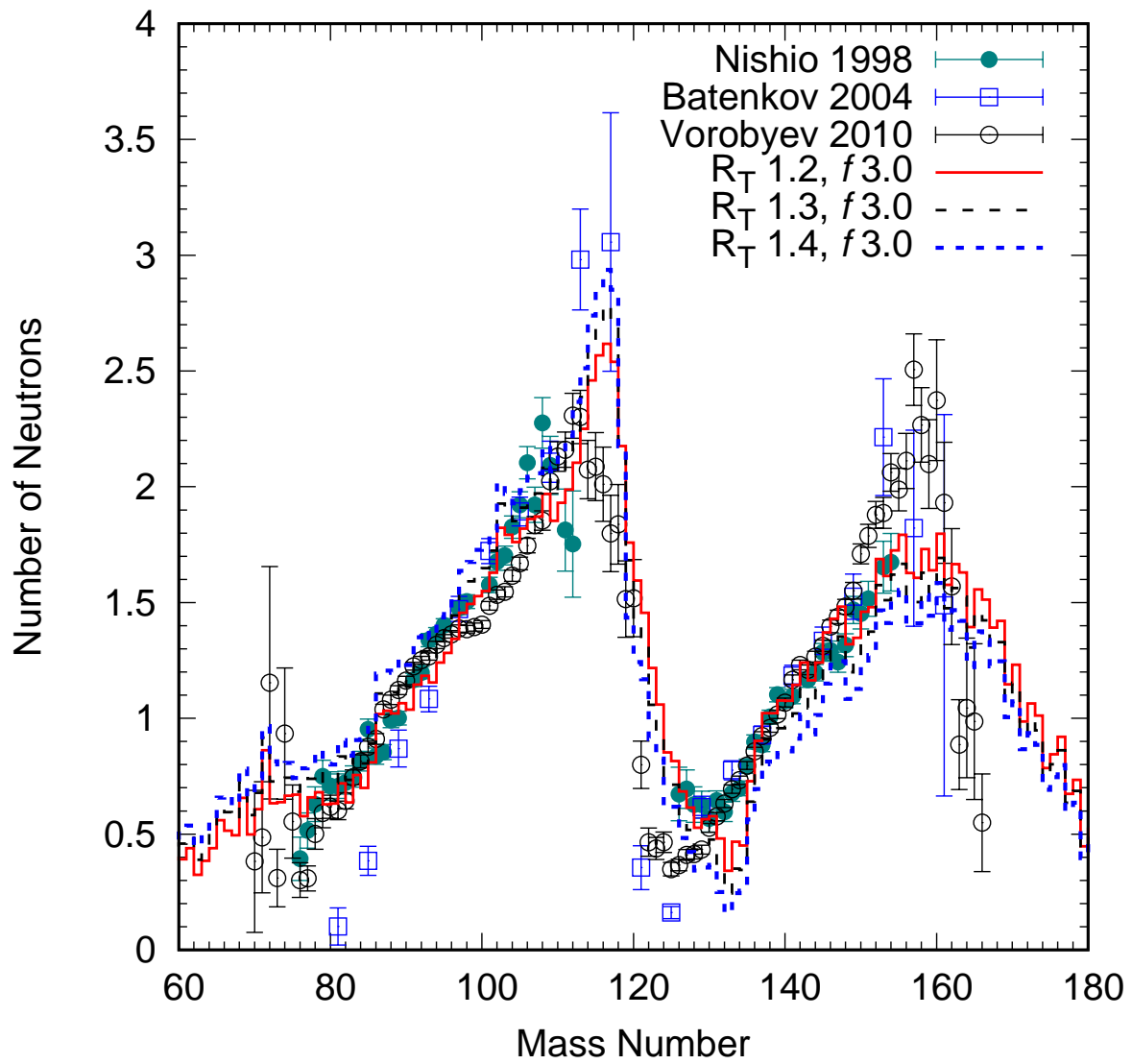


Figure 5 The calculated $\bar{\nu}(A)$ with the scaling factors $f = 3.0$ and the anisothermal parameter $R_T = 1.2, 1.3$ and 1.4 .

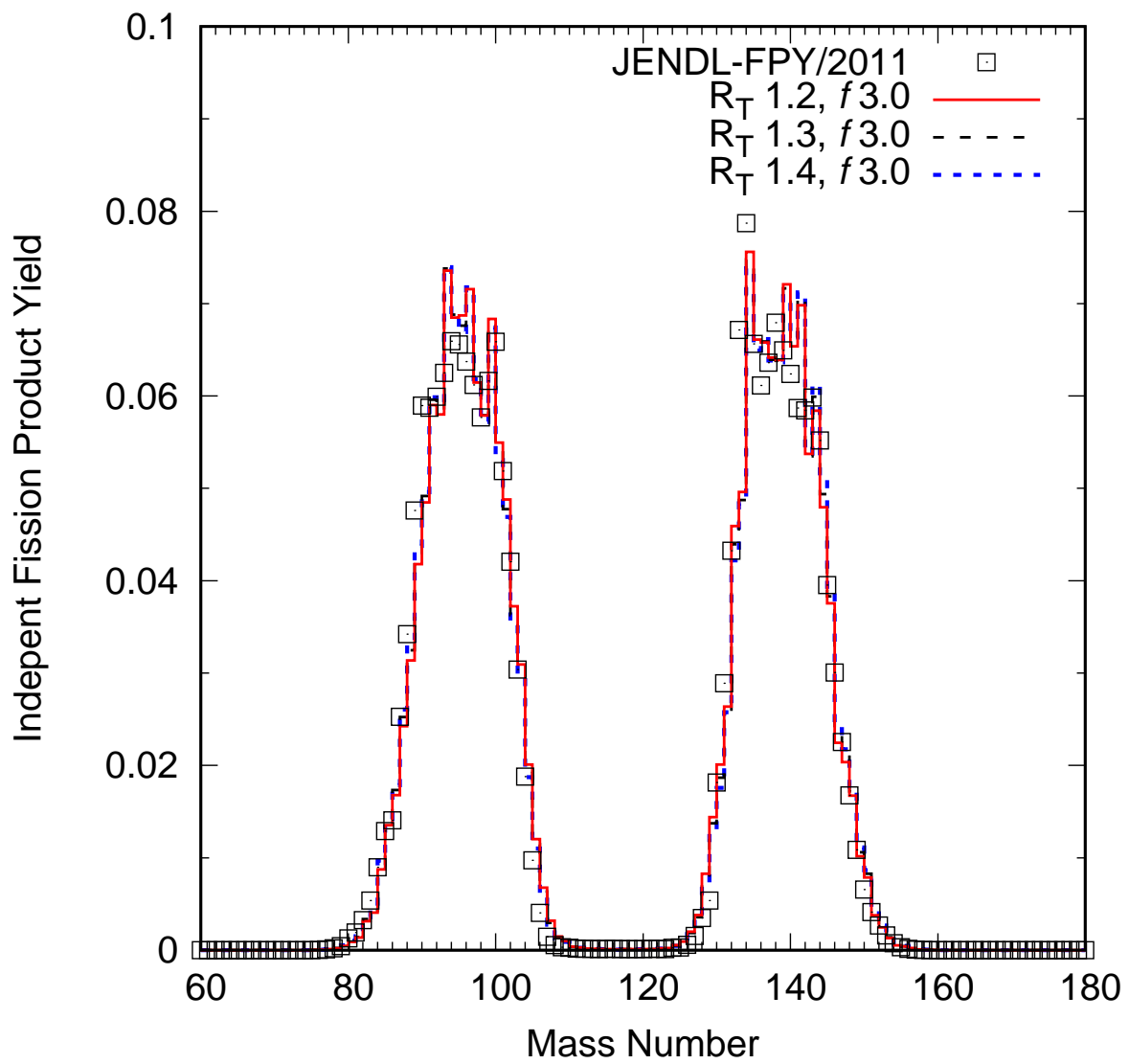


Figure 6 The calculated post-neutron distribution of fission products $Y_I(A)$ with the scaling factor $f = 3.0$ and the anisothermal parameter $R_T = 1.0, 1.2$ and 1.4 .

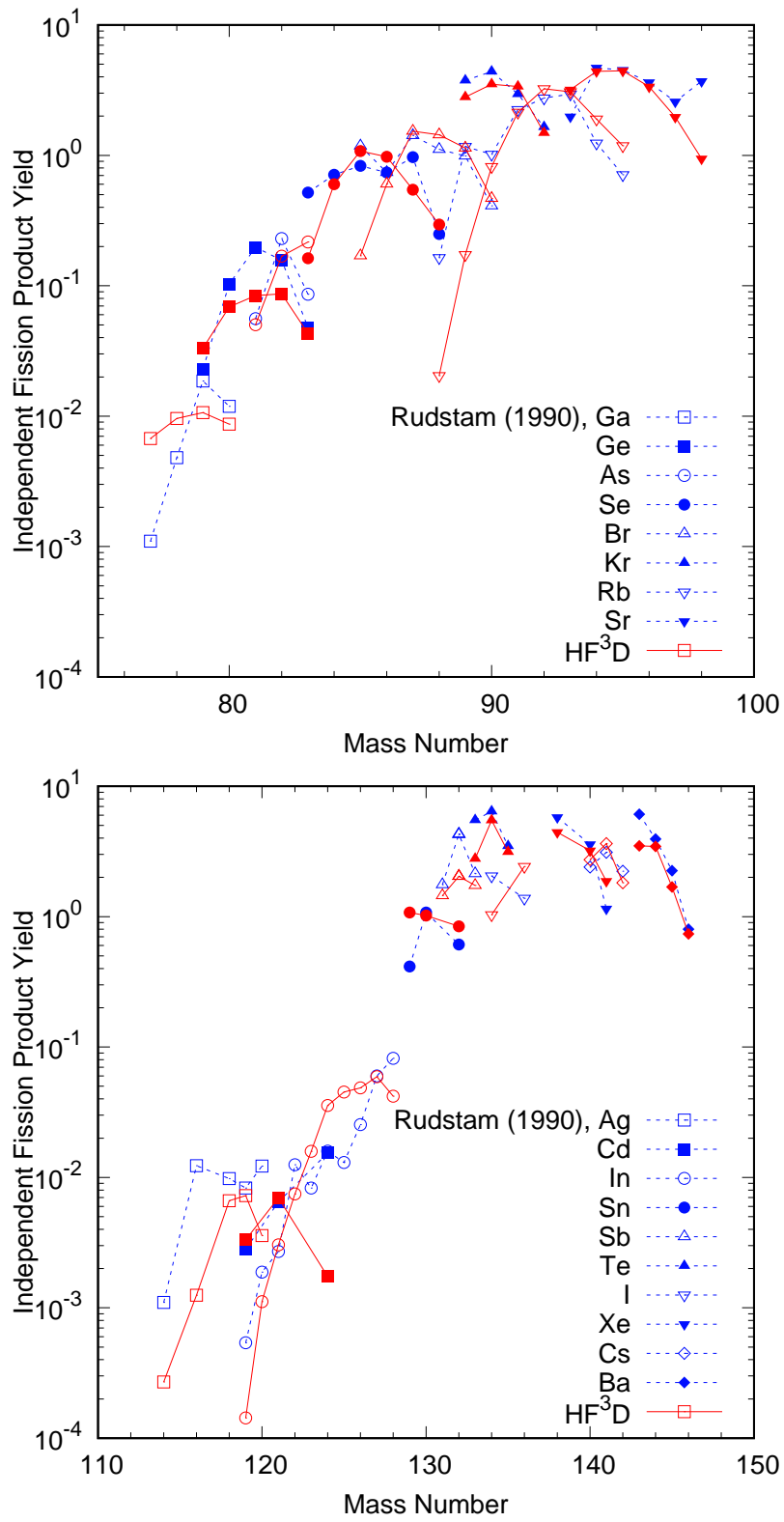


Figure 7 Comparison of the calculated independent yield $Y_I(Z, A)$ with the experimental data reported

by Rudstam *et al.*⁶¹

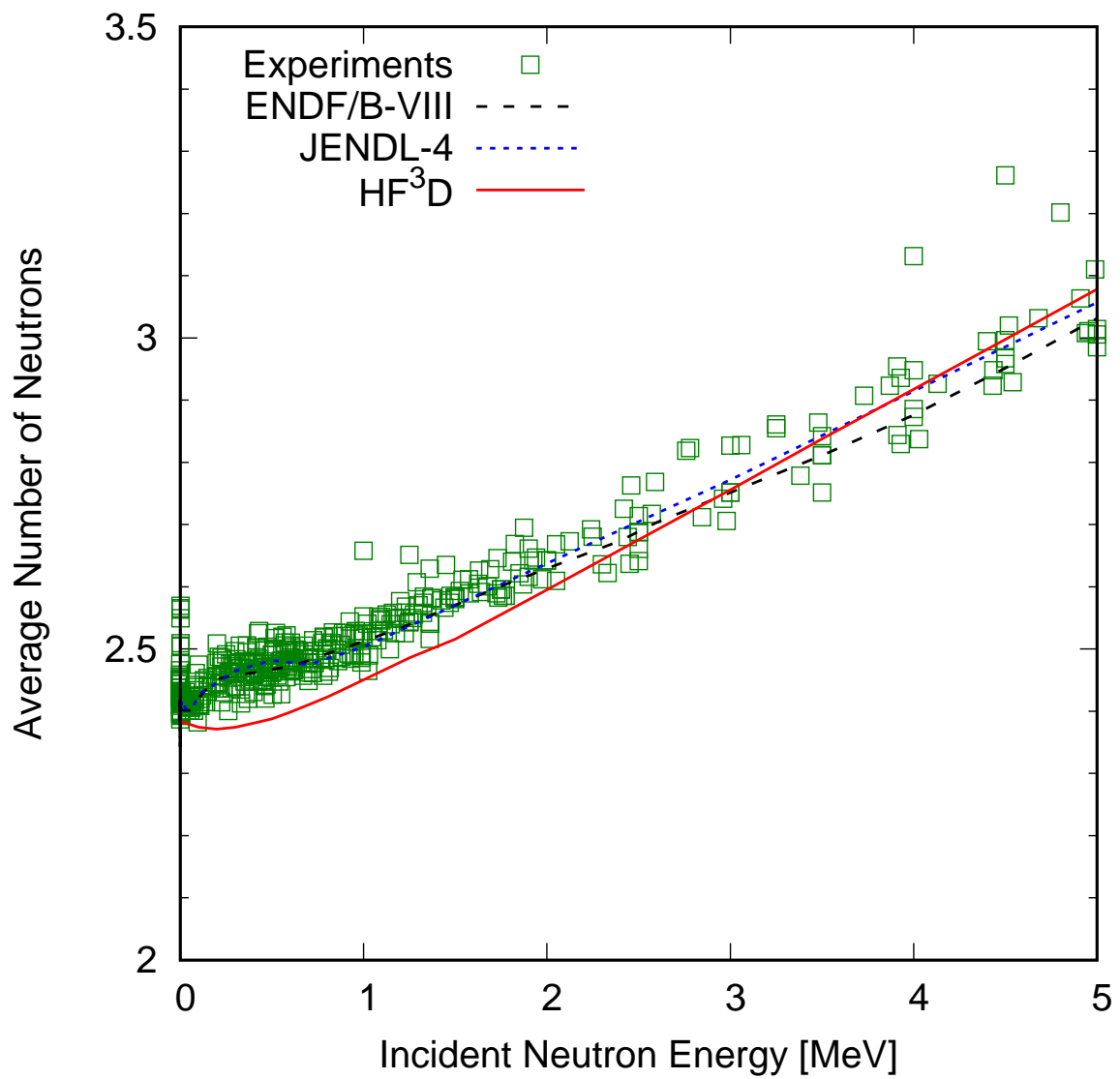


Figure 8 The calculated average number of prompt neutrons $\bar{\nu}$ comparing with the evaluated $\bar{\nu}$ in ENDF/B-VIII (dashed line) and JENDL-4 (dotted line), and experimental data taken from the EXFOR databaes.

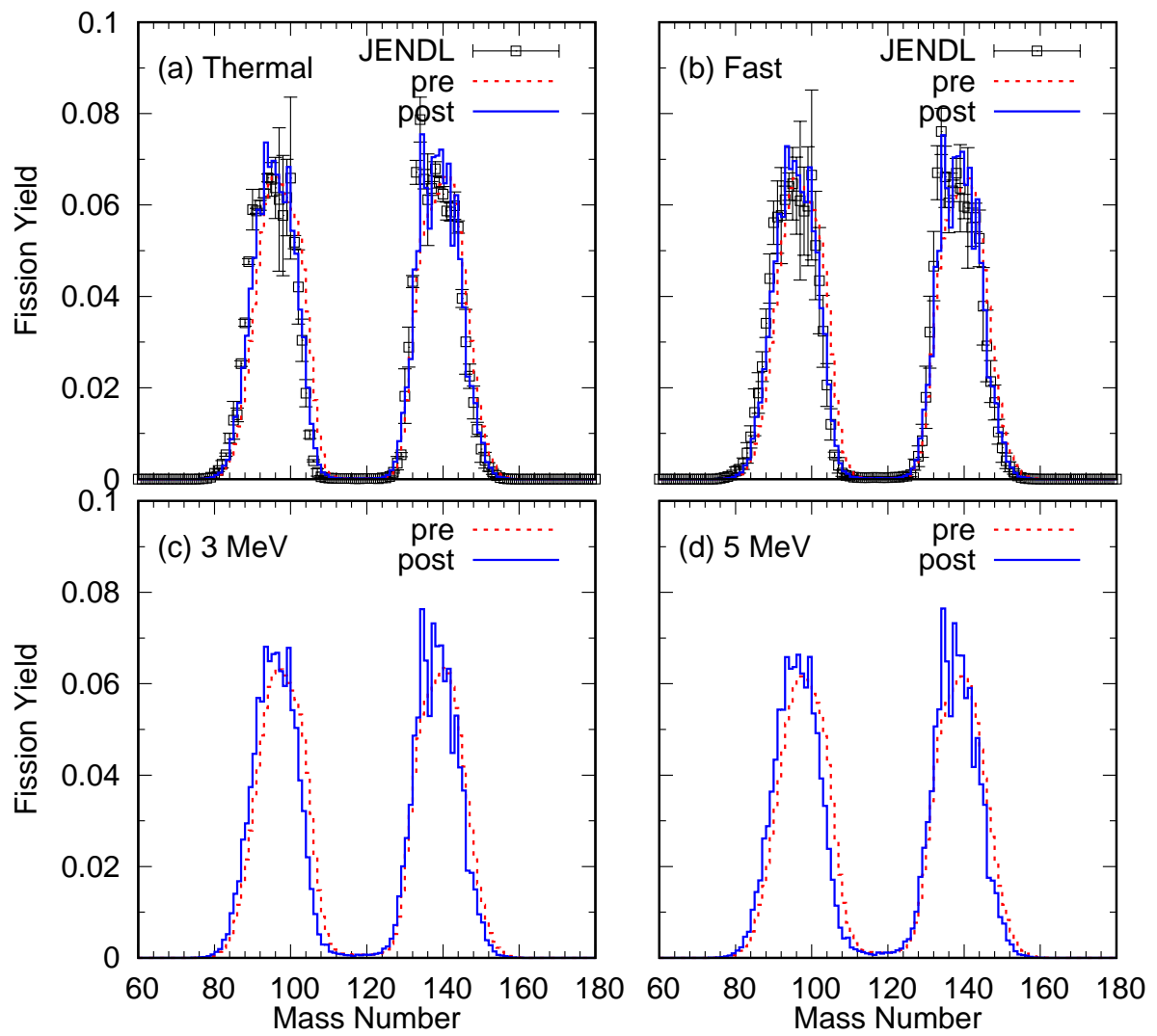


Figure 9 The calculated $Y_I(A)$ at (a) thermal, (b) fast energy, (c) 3, and (d) 5 MeV. The evaluated $Y_I(A)$ in JENDL/FPY-2011 at the thermal and fast energies are also depicted in the top panels.

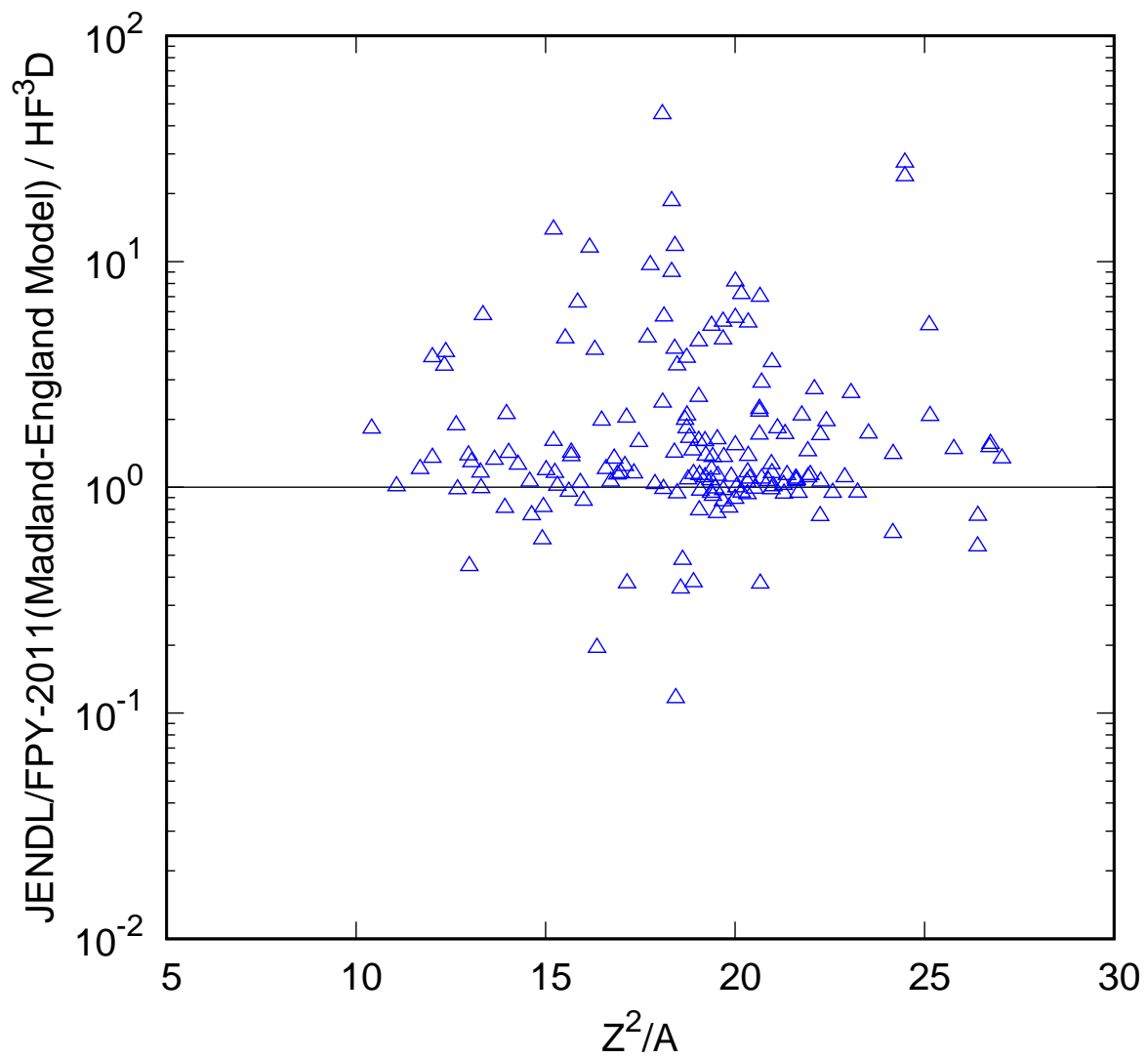


Figure 10 The ratio of the Madland-England model to the Hauser-Feshbach calculation by HF³D for all possible fission products containing the metastable state.

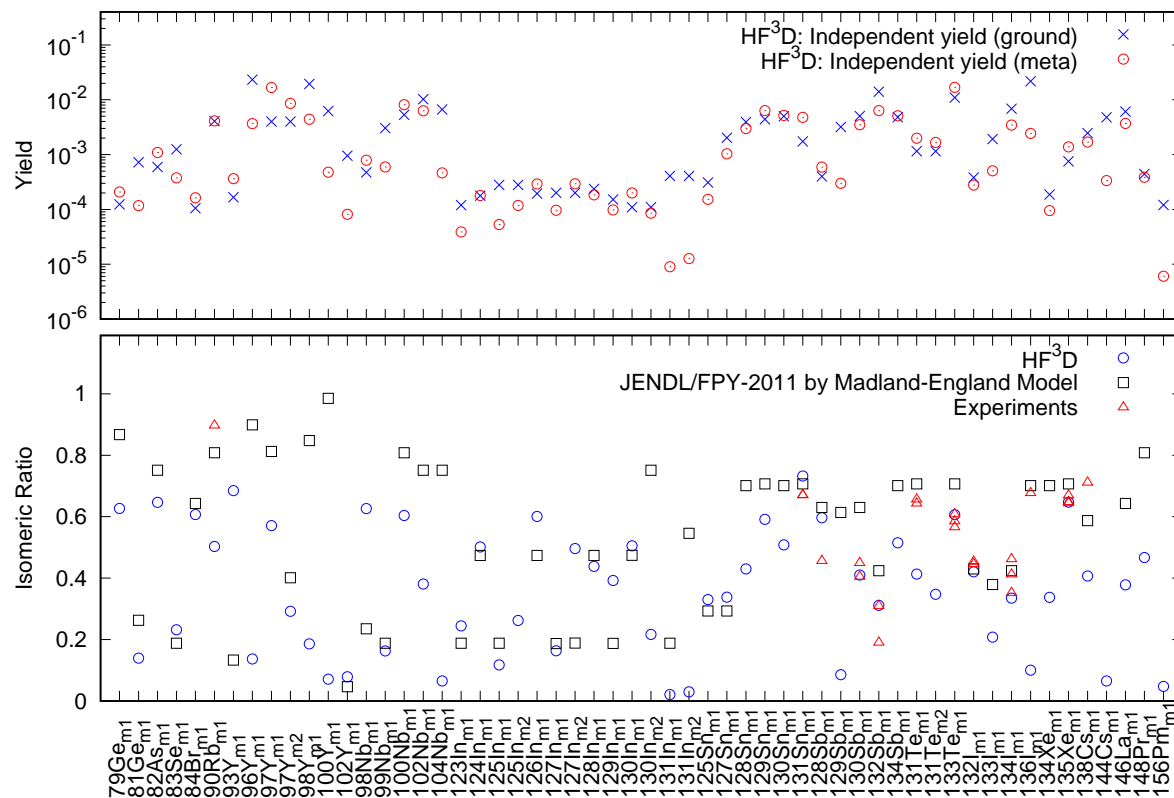


Figure 11 Calculated fractional independent yields (upper panel) and IRs (bottom panel) for the nuclides that have the ground state yield of greater than 1×10^{-4} . The IRs are shown together with JENDL/FPY-2011 data compiled by the Madland-England model, and some experimental data. The first and the second isomeric states are denoted by the subscript.

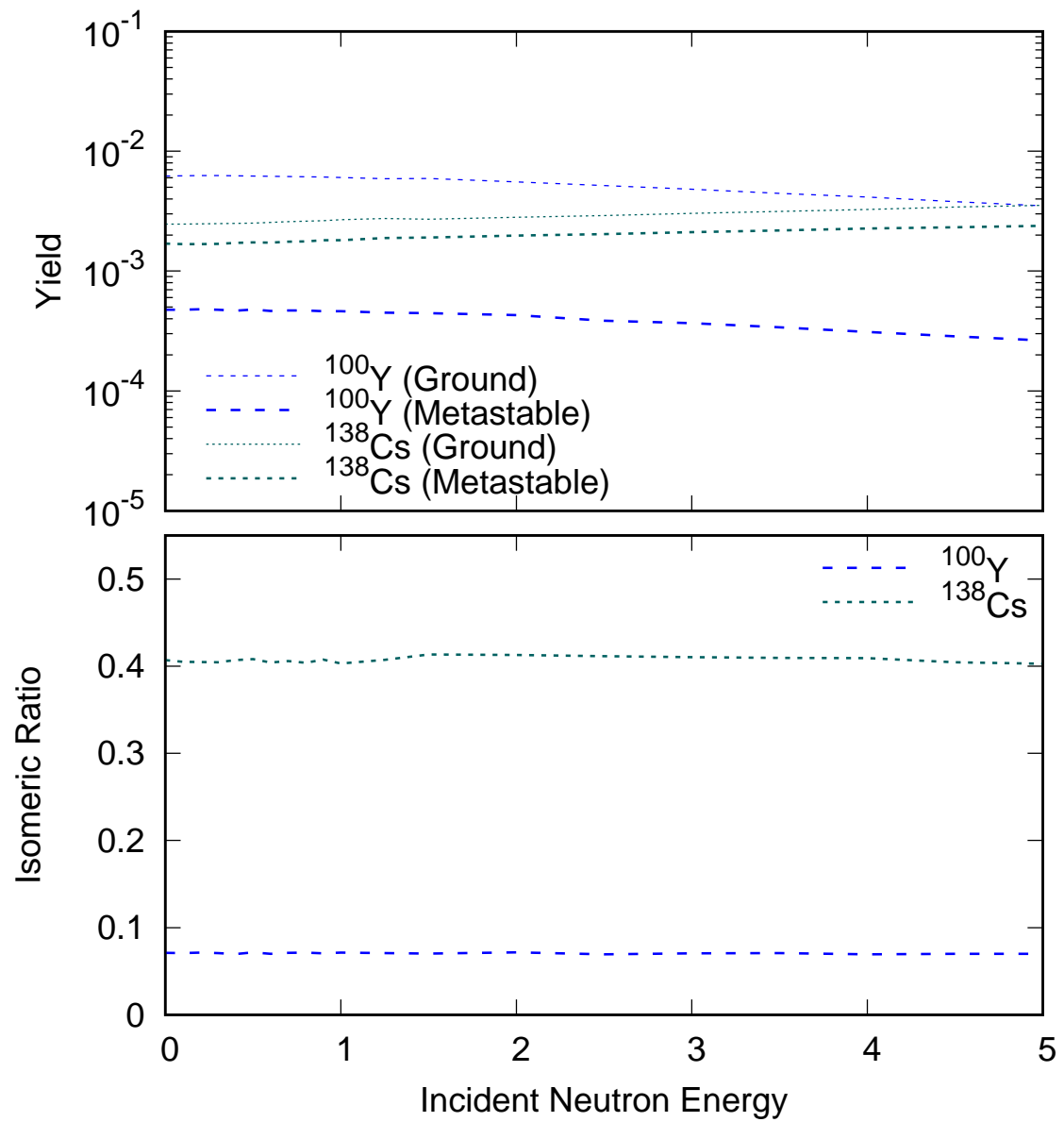


Figure 12 Energy dependence of ground and metastable state yield (top frame) and isomeric ratio (bottom frame) of ^{100}Y and ^{138}Cs .